Experimental and theoretical study of longitudinally monomode vectorial solid-state lasers

Marc Brunel,* Olivier Emile, Mehdi Alouini, Albert Le Floch, and Fabien Bretenaker
Laboratoire d'Electronique Quantique–Physique des Lasers, Unité Mixte de Recherche du Centre National de la Recherche Scientifique No. 6627, Université de Rennes I, Campus de Beaulieu, F-35042 Rennes Cedex, France
(Received 5 March 1998)

The dynamics of a quasi-isotropic continuous-wave solid-state laser sustaining the oscillation of two orthogonally polarized eigenstates is experimentally investigated. A set of phase-sensitive vectorial Maxwell-Bloch equations is developed to describe theoretically the evolution of such a laser. Different temporal behaviors for the output intensities are observed, depending on the relative amounts and orientations of the phase and loss anisotropies and on the frequency of relaxation oscillations. Namely, the frequency locking of the two orthogonally linearly polarized eigenstates is shown to lead to a surprising pulsed mode-locked oscillation regime. In addition, for different values of the parameters, other peculiar operation regimes are found, such as cw circularly polarized, double-pulsed, or triple-pulsed output intensities. These experimental results, obtained using a diode-pumped Nd:YAG (YAG denotes yttrium aluminum garnet) laser, are well confirmed by the theoretical model. [S1050-2947(99)07601-5]

PACS number(s): 42.55.Ah; 42.60.Fc; 42.25.Ja

I. INTRODUCTION

Monomode solid-state lasers are usually described theoretically by the so-called rate equations, which yield the dynamical evolutions of the photon number and of the population inversion in a laser cavity. Derived by Statz and de Mars [1], this formalism arises from a semiclassical description of the atom-field system, where the atomic polarization is adiabatically eliminated. It has proven satisfactory to predict the transient—spiking, relaxation oscillations—and steady-state outputs of monomode solid-state lasers. When two or more longitudinal laser modes oscillate, extensions of the model have taken the spatial hole-burning effect into account [2,3], but the atom-field interaction has kept its scalar nature, hence applying only to lasers oscillating in a single polarization eigenstate. However, quasi-isotropic solid-state lasers, which may sustain the oscillation of two orthogonally polarized eigenstates in the same longitudinal mode, have recently been the subject of widespread research, due to their potential applications in Doppler velocimetry, vibrometry, and optical microwave systems [4–11]. Indeed, this two-eigenstate oscillation regime has been shown to be permitted by the relatively low value of the coupling constant between orthogonally polarized eigenstates in solid-state lasers [12]. Moreover, peculiar self-pulsing behaviors have recently been observed using these two-frequency lasers [13,14]. In Ref. [14], it was observed that a frequency locking between the two cold-cavity eigenstates due to a transverse loss anisotropy was responsible for the appearance of a monomode pulsed output. Namely, this unexpected phenomenon appears when the relaxation oscillation frequency of the laser falls within the locking region. But, to date, no theoretical model taking cold-cavity eigenstate locking into account has led to predictions close to these experimental observations. Although a vectorial model, i.e., a model where the transverse dependence of the field-atom interaction is taken into account, has been developed to describe polarization instabilities in strongly multimode fiber lasers [15,16], it has not been experimentally investigated in the case of longitudinally monomode lasers, especially when one introduces transverse loss anisotropy, i.e., a locking mechanism between the two polarization eigenstates. Of course, to describe such locking behaviors, phase-sensitive interactions have to be taken into account, as in Refs. [15, 16] and in the case of the dynamics of two-longitudinal mode [17] or three-transverse mode [18] lasers.

The aim of this paper is consequently twofold. First, we manage to derive a set of phase-sensitive Maxwell-Bloch equations which takes the transverse nature of the atom-field interaction into account and includes the crossed phase and loss anisotropies of the cavity. Second, the predictions of this model obtained by numerical integration of the differential equations of evolution of the laser are compared with the experimental behavior of a longitudinally monomode quasi-isotropic diode-pumped Nd:YAG (YAG denotes yttrium aluminum garnet) laser. Original intensity and polarization dynamics are emphasized. This paper is organized as follows. Section II is devoted first to the calculation of the cold-cavity eigenstates (Sec. II A). Second, the derivation of the differential equations relating the amplitudes and phases of the two electromagnetic field eigenstates and the population inversion in the active medium is performed, starting from the density matrix formalism (Sec. II B). The comparison between the results of the numerical integration of these equations and the corresponding experimental results is presented in Sec. III. After a brief description of the experimental setup (Sec. III A), the dynamics of the two-eigenstate laser is explored, with full attention paid to the magnitude of the locking region with respect to the relaxation oscillation frequency (Sec. III B). Particular attention is paid to the application of these dynamics to the development of short pulse monomode lasers without *Q* switch. The results, as well as the perspectives of this work, are then summarized in Sec. IV.

*Electronic address: brunel@univ-rennesl.fr

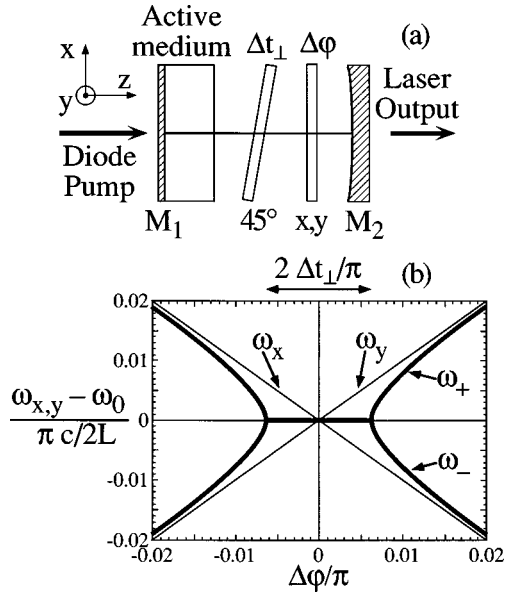

FIG. 1. (a) Experimental arrangement. Active medium: Nd:YAG crystal. $\Delta\varphi$:x-y phase anisotropy. $\Delta t_\perp$: slightly tilted étalon, ensuring longitudinally monomode oscillation and creating a crossed loss anisotropy. (b) Evolution of the angular eigenfrequencies ω_+ and ω_- of the cold-cavity eigenstates versus phase anisotropy $\Delta\varphi$. $\omega_0=(\omega_x+\omega_y)/2$ is the average laser angular frequency. Notice the locking region $\Delta\omega_L=c\Delta t_\perp/L$.

II. THEORETICAL MODEL

A. Calculation of the laser eigenstates

Let us derive the cavity eigenstates of a Fabry-Perot laser closed by two mirrors M_1 and M_2 and containing phase and loss anisotropies, as depicted in Fig. 1(a). To this aim, we recall the calculation of the Jones matrix M corresponding to the propagation of the light electromagnetic field for one round-trip inside the cavity. We consider both a linear phase retardance $\Delta\varphi$ between the x and y polarization directions and a small linear loss anisotropy $\Delta t_\perp$ not aligned with $\Delta\varphi$. For simplicity, we choose the orientation of the low-loss axis at $+45°$ with respect to the x and y axes. The active medium is supposed to be isotropic. Starting from the middle of the cavity, the matrix M is then

$$M=\begin{bmatrix}\exp(-i\Delta\varphi) & 0\\ 0 & \exp(i\Delta\varphi)\end{bmatrix}\begin{bmatrix}1 & \Delta t_\perp\\ \Delta t_\perp & 1\end{bmatrix}. \quad (1)$$

The resolution of the resonance condition $M\mathbf{E}=\lambda\mathbf{E}$, where $\mathbf{E}$ is the electromagnetic field amplitude and λ the corresponding eigenvalue, yields the laser eigenvectors and eigenfrequencies. With the phase anisotropy alone, i.e., when $\Delta t_\perp=0$, the laser eigenstates are linearly polarized along the x and y axes, with angular frequencies ω_x and ω_y, respectively. Their difference is $\omega_y-\omega_x=c\Delta\varphi/L$, where c is the velocity of light and L the optical length of the cavity, as shown by the straight lines in Fig. 1(b). Now, in the case where a small loss anisotropy $\Delta t_\perp \ll 1$ exists, the eigenstates become slightly elliptical and a frequency locking region $\Delta\omega_L=c\Delta t_\perp/L$ appears. One can then distinguish between two operating regimes. On the one hand, when $|\omega_y-\omega_x|<\Delta\omega_L$, the two elliptical eigenstates lock to the same eigenfrequency and experience different losses. On the other hand, for $|\omega_y-\omega_x|>\Delta\omega_L$, the two eigenstates are also elliptical, exhibit the same losses, but their angular frequencies ω_+ and ω_- are no longer degenerate, leading to a beat frequency ω_b given by

$$\omega_b\equiv\omega_+-\omega_-\approx(\omega_y-\omega_x)[1-\Delta\omega_L^2/(\omega_y-\omega_x)^2]^{1/2}. \quad (2)$$

The cold-cavity eigenstates that we have just derived, and in particular their beat frequency given by Eq. (2), will serve as a guideline for the physical discussion of the results. However, quantitative predictions of the laser behavior can be obtained only if we take the role of the active medium into account, as is now going to be performed.

B. Derivation of the coupled field-atom equations

To fully describe theoretically the behavior of the laser, we need a set of Maxwell-Bloch equations to predict the temporal evolution of the field-atom system, taking the cold-cavity anisotropies, the vectorial nature of the electromagnetic field [15,16], and phase-sensitive interactions [15–18] into account. First, since in the experiments described in Sec. III the active medium is located near one of the mirrors of the cavity and is much thinner than the beat length between the two eigenstates, we can neglect spatial hole-burning effects. This allows us to withdraw the spatial dependence of the electromagnetic field and to write the associated electric field $\mathbf{E}$ in the following manner:

$$\mathbf{E}(t)=\tfrac{1}{2}\{E_x\exp[-i(\omega_x t+\varphi_x)]\hat{\mathbf{x}}+E_y\exp[-i(\omega_y t+\varphi_y)]\hat{\mathbf{y}}\}+\text{c.c.}, \quad (3)$$

where E_x and φ_x (respectively, E_y and φ_y) are the time-dependent real amplitude and phase of the x-polarized (respectively y-polarized) component of the field in the active medium and where $\hat{\mathbf{x}}$ and $\hat{\mathbf{y}}$ are unit vectors along the x and y directions, i.e., perpendicular to the laser axis z. In the slowly varying amplitude and phase approximation, and if in a first step we neglect the loss anisotropy $\Delta t_\perp$, we then obtain the following equations of evolution of the fields [15]:

$$\left(\partial_t+\frac{\Gamma_x}{2}\right)[E_x\exp(-i\varphi_x)]=\frac{i\omega_x}{2\varepsilon_0}\int_0^{2\pi}\eta_x(\theta,t)d\theta, \quad (4a)$$

$$\left(\partial_t+\frac{\Gamma_y}{2}\right)[E_y\exp(-i\varphi_y)]=\frac{i\omega_y}{2\varepsilon_0}\int_0^{2\pi}\eta_y(\theta,t)d\theta, \quad (4b)$$

where Γ_x and Γ_y are the intensity loss coefficients along the x and y directions and where η_x and η_y are the slowly varying complex amplitudes of the x- and y-polarized components of the dipole moments induced by the laser transition. As in Ref. [15], we suppose that these terms depend on the orientation θ of the dipole of the considered emitting atom with respect to the x axis. Although in the case we consider here of an emitting ion embedded in a crystalline matrix (Nd:YAG) one should consider the environment of each emitting ion, we still follow the approximations used in Ref. [15] for the case of neodymium ions in a glass. We will indeed see in the experimental section that (i) the model obtained is in good agreement with experiments and (ii) the

same laser behaviors are obtained for glass active media as well as for crystal active media, emphasizing the low importance of the emitting ion environment on the considered physics.

As in Ref. [15], we obtain expressions for the source terms η_x and η_y in Eqs. (4) from the time evolution of the density matrix elements and by adiabatic elimination of the optical coherences between the two laser levels, leading to

$$\eta_x = -\frac{T_s\mu^2}{4\hbar}(i\alpha_x+\tilde{\alpha}_x)D(\theta,t)\{E_x\exp(-i\varphi_x)(1+\cos 2\theta) + E_y\exp[-i(\omega_y-\omega_x)t-i\varphi_y]\sin 2\theta\}, \quad (5a)$$

$$\eta_y = -\frac{T_s\mu^2}{4\hbar}(i\alpha_y+\tilde{\alpha}_y)D(\theta,t)\{E_y\exp(-i\varphi_y)(1-\cos 2\theta) + E_x\exp[-i(\omega_x-\omega_y)t-i\varphi_x]\sin 2\theta\}, \quad (5b)$$

where T_s is the lifetime of optical coherences, $\alpha_j = 1/[1+T_s^2(\omega-\omega_j)^2]$ and $\tilde{\alpha}_j = T_s(\omega-\omega_j)\alpha_j$ for $j=x,y$, ω is the center frequency of the transition, μ is the magnitude of the dipole moment of the considered transition, and $D(\theta,t)$ is the population inversion. From the density matrix equations, we also obtain the equation of evolution of this population inversion, leading to

$$\begin{aligned}(\partial_t+\gamma_\parallel)D(\theta,t) = \sigma &- \zeta D(\theta,t)[\alpha_x E_x^2(1+\cos 2\theta) \\ &+ \alpha_y E_y^2(1-\cos 2\theta)] \\ &- \zeta D(\theta,t)[(\alpha_x+\alpha_y)\cos\Psi \\ &+ (\tilde{\alpha}_x-\tilde{\alpha}_y)\sin\Psi]E_xE_y\sin 2\theta, \end{aligned} \quad (6)$$

where

$$\zeta = \frac{T_s\mu^2}{2\hbar^2}, \quad (7)$$

$$\Psi = (\omega_x-\omega_y)t+\varphi_x-\varphi_y, \quad (8)$$

and where $\gamma_\parallel$ is the decay time of the population inversion and σ is the pumping rate. Since in our experiments the pump laser is completely depolarized by its propagation through the fiber, we consider the pumping process to be isotropic, i.e., we suppose that σ does not depend on θ.

If now we introduce Eqs. (5) in the right-hand side of Eqs. (4), we can see that the following angular Fourier components D_0, D_1, and D_2 of the population inversion $D(\theta,t)$ appear:

$$D_0(t) = \frac{1}{2\pi}\int_0^{2\pi} d\theta\, D(\theta,t), \quad (9a)$$

$$D_1(t) = \frac{1}{2\pi}\int_0^{2\pi} d\theta\, \cos 2\theta D(\theta,t), \quad (9b)$$

$$D_2(t) = \frac{1}{2\pi}\int_0^{2\pi} d\theta\, \sin 2\theta D(\theta,t). \quad (9c)$$

The equations of evolution of the field then become

$$\left(\partial_t+\frac{\Gamma_x}{2}\right)E_x = \kappa\alpha_x E_x(D_0+D_1) + \kappa(\alpha_x\cos\Psi+\tilde{\alpha}_x\sin\Psi)E_yD_2, \quad (10a)$$

$$\left(\partial_t+\frac{\Gamma_y}{2}\right)E_y = \kappa\alpha_y E_y(D_0-D_1) + \kappa(\alpha_y\cos\Psi-\tilde{\alpha}_y\sin\Psi)E_xD_2, \quad (10b)$$

$$\partial_t\varphi_x = \kappa\tilde{\alpha}_x(D_0+D_1) - \kappa(\alpha_x\sin\Psi-\tilde{\alpha}_x\cos\Psi)\frac{E_y}{E_x}D_2, \quad (10c)$$

$$\partial_t\varphi_y = \kappa\tilde{\alpha}_y(D_0-D_1) + \kappa(\alpha_y\sin\Psi+\tilde{\alpha}_y\cos\Psi)\frac{E_x}{E_y}D_2, \quad (10d)$$

where

$$\kappa = \frac{\omega T_s\mu^2}{8\hbar\varepsilon_0}. \quad (11)$$

Notice that contrary to Ref. [15], we have explicitly developed the terms containing the phase Ψ in our equations and we will apply the model to a strictly longitudinally monomode laser in Sec. III, devoted to the experimental results. The terms containing the phase Ψ describe phase-sensitive interactions and will lead to the relevant phase locking phenomena in conjunction with the cold-cavity anisotropies. Finally, we derive the equations of evolutions of the Fourier components D_0, D_1, and D_2 [see Eqs. (9)] of the population inversion thanks to Eq. (6), leading to

$$\dot{D}_0 = \gamma_\parallel(P_0-D_0) - \zeta[\alpha_x(D_0+D_1)I_x+\alpha_y(D_0-D_1)I_y] - \zeta[(\alpha_x+\alpha_y)\cos\Psi+(\tilde{\alpha}_x-\tilde{\alpha}_y)\sin\Psi]D_2\sqrt{I_xI_y}, \quad (12a)$$

$$\dot{D}_1 = -\gamma_\parallel D_1 - \zeta[\alpha_x(D_1+D_0/2)I_x+\alpha_y(D_1-D_0/2)I_y], \quad (12b)$$

$$\dot{D}_2 = -\gamma_\parallel D_2 - \zeta[\alpha_xD_2I_x+\alpha_yD_2I_y] - \zeta[(\alpha_x+\alpha_y)\cos\Psi+(\tilde{\alpha}_x-\tilde{\alpha}_y)\sin\Psi]D_0/2\sqrt{I_xI_y}, \quad (12c)$$

where we have kept only the first three terms D_0, D_1, and D_2 in the Fourier expansion of $D(\theta,t)$, where P_0 is the pumping rate, and where $I_x=E_x^2$ and $I_y=E_y^2$. Using these notations and after having reintroduced the loss anisotropy $\Delta t_\perp$ which creates the locking region [see Fig. 1(b)], the field equations (10) finally become

$$\dot{I}_x = -\Gamma_xI_x+\Delta\omega_L\sqrt{I_xI_y}\cos\Psi+2\kappa\alpha_x(D_0+D_1)(I_x+\varepsilon_x) + 2\kappa(\alpha_x\cos\Psi+\tilde{\alpha}_x\sin\Psi)D_2\sqrt{I_xI_y}, \quad (13a)$$

$$\dot{I}_y = -\Gamma_yI_y+\Delta\omega_L\sqrt{I_xI_y}\cos\Psi+2\kappa\alpha_y(D_0-D_1)(I_y+\varepsilon_y) + 2\kappa(\alpha_y\cos\Psi-\tilde{\alpha}_y\sin\Psi)D_2\sqrt{I_xI_y}, \quad (13b)$$

$$\dot{\Psi}=\omega_x-\omega_y-2\Delta\omega_L(\sqrt{I_x/I_y}+\sqrt{I_y/I_x})\sin\Psi + \kappa[\tilde{\alpha}_x(D_0+D_1)-\tilde{\alpha}_y(D_0-D_1)] - \kappa[(\alpha_x\sin\Psi-\tilde{\alpha}_x\cos\Psi)\sqrt{I_y/I_x} - (\alpha_y\sin\Psi+\tilde{\alpha}_y\cos\Psi)\sqrt{I_x/I_y}]D_2, \quad (13c)$$

where ε_x and ε_y are small quantities which hold for spontaneous emission. Finally, we define the relative excitation rate η by

$$\eta=4\kappa P_0(\Gamma_x/\alpha_x+\Gamma_y/\alpha_y)^{-1}. \quad (14)$$

In the following, we use Eqs. (12) and (13) to simulate the behavior of the laser. This set of six coupled nonlinear differential equations is numerically integrated using a fourth-order Runge-Kutta algorithm [19] and using the parameters given by the experiment.

III. EXPERIMENTAL RESULTS

A. Experimental arrangement

The longitudinally pumped laser used in the experiments is schematized in Fig. 1(a). The active medium is a 1.1-mm-long crystal of 1 at. % doped Nd:YAG. One of its ends [see M_1 in Fig. 1(a)] is highly transmitting ($T>95\%$) at the pump wavelength, i.e., 809 nm, and highly reflecting ($R>99.5\%$) at 1064 nm. The resonator is $L=385$ mm long and is closed with a 500-mm radius of curvature concave mirror M_2 with transmission $T=1\%$ at 1064 nm, which serves as the output coupler. The pump laser is a fiber-coupled laser diode whose emission wavelength matches the absorption peak of Nd:YAG at 809 nm. The end of the fiber is butted against the input face of the laser crystal. A 1.5-mm-diam aperture is placed against the output mirror to ensure a single transverse mode oscillation. A continuously adjustable linear phase retardance $\Delta\varphi$ between the x and y polarization directions is created by two intracavity quarter-wave plates whose neutral axes are not aligned. The two eigenstates are forced to oscillate in a single longitudinal mode thanks to an uncoated 2-mm-thick silica plate, which acts as an étalon. Indeed, we focus here on the dynamics of the two eigenstates of a longitudinally monomode laser, contrary to previous works [16,20,21] which dealt with a great number of simultaneously oscillating longitudinal modes. Moreover, owing to the Fresnel reflections on both faces of this étalon, whose normal axis is tilted with respect to the propagation axis of the cavity, we use this étalon to create and control the loss anisotropy $\Delta t_\perp \ll 1$.

For the purpose of the analysis, the laser output is passed through a polarizer followed by an optical isolator, and separated into two beams. One part is sent to a 1.5-GHz confocal Fabry-Perot interferometer in order to check that the laser is longitudinally monomode. The other part is focused on a 200-MHz bandwidth InGaAs photodiode. The electrical signal obtained is then monitored thanks to an oscilloscope and a spectrum analyzer. This experimental arrangement allows us to check the output intensity and polarization evolutions when the intracavity parameters are modified by slight adjustment of the phase and loss anisotropies.

In order to compare the experimental observations with the predictions provided by the theoretical model, we feed the differential equations with the values of the different parameters given by the experiment. These data are summarized hereafter. With the above-mentioned elements inside the cavity, the laser is chosen to operate at an excitation ratio $\eta=2.0$ (we then measure an output power of 20 mW). The analysis of the low-frequency intensity spectrum yields the relaxation oscillation frequency [22]. At this excitation level, it is measured to be $\omega_r/2\pi=65$ kHz. In the Nd:YAG lasers we consider here, the spontaneous emission lifetime $1/\gamma_\parallel=230\ \mu$s of the upper level of the laser transition is much longer than the cavity lifetime. We can consequently use the well-known relation [23,24]

$$\omega_r^2=(\eta-1)\Gamma_x\gamma_\parallel, \quad (15)$$

leading then to the loss rate of the cavity $\Gamma_x=3.8\times10^7\ \mathrm{s}^{-1}$. Of course, the low-frequency intensity spectrum also exhibits very-low-frequency ($\approx$15 kHz) structures associated with antiphase dynamics of the two eigenstates [20]. In the following, we experimentally investigate different dynamical behaviors associated with the existence of the transverse loss anisotropy locking mechanism, and consequently overlook this antiphase dynamics. Besides, the coherence lifetime is taken equal to $T_s=80$ ps [15] and the average detuning is chosen to be $\omega_0/2\pi=1$ MHz in the calculations. The quarter-wave plates and the étalon are mounted on micrometric positioning stages, permitting us to finely tune the values of the phase and loss anisotropies. Nevertheless, the absolute values of these small phase and loss anisotropies are difficult to measure directly. Thus, in the following, these parameters are adjusted in the calculations to meet the corresponding experimental results. Depending on these quantities, various intensity dynamics are observed, as is now described.

B. Investigation of the laser dynamics

Among the numerous intensity behaviors obtained both theoretically and experimentally when changing the intracavity anisotropies, we choose to focus our study on the parameter regions where uncommon features appear. Numerical integration of the set of differential equations developed in Sec. II evidences three main regions, which lead to different singular intensity and phase dynamics. These regions are defined by the relative magnitude of the locking region $\Delta\omega_L$ with respect to the relaxation oscillation frequency ω_r and the frequency difference $\omega_+-\omega_-$ between the two cold-cavity eigenstates of the laser. Within the framework of this classification, the laser intensity behavior is consequently studied in each region when the beat frequency $\omega_b=\omega_+-\omega_-$ is varied. Experimentally, this is obtained by rotating one of the quarter-wave plates, hence varying the phase anisotropy $\Delta\varphi$.

1. $\Delta\omega_L$, $\omega_r \ll \omega_y-\omega_x$

We first consider the case where the laser has almost no loss anisotropy, i.e., when the locking region is almost as small as the relaxation oscillation frequency $\omega_r/2\pi=65$ kHz. We start from $\omega_b \gg \omega_r$. We detect experimentally

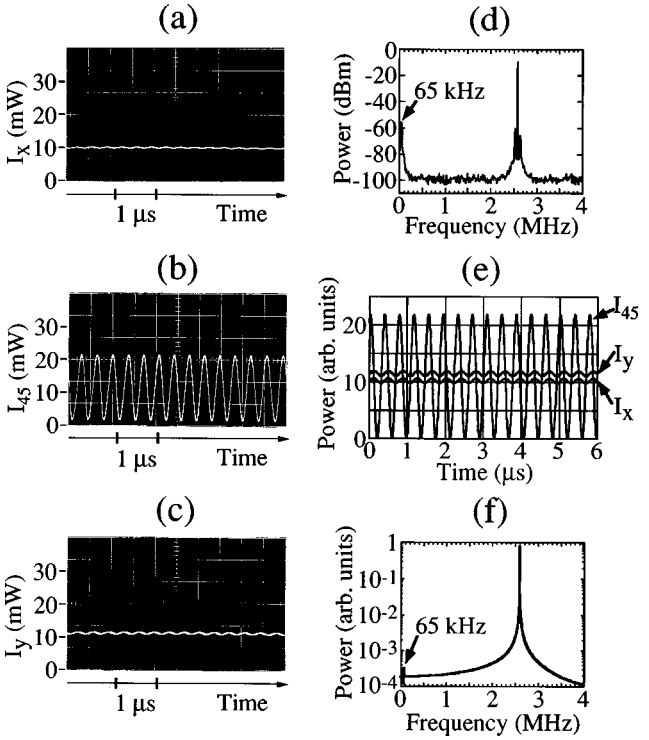

FIG. 2. (a)–(c) Experimental time evolution of the laser output power observed behind a polarizer oriented (a) along the x axis, (b) at 45° of the x and y axes, and (c) along the y axis, when $|\omega_y - \omega_x| > \Delta\omega_L$. (d) Experimental power spectrum corresponding to (b). (e), (f) Corresponding theoretical results obtained with $\Gamma_y/0.971 = \Gamma_x = 3.8\times10^7\ s^{-1}$, $1/\gamma_\parallel = 230\ \mu s$, $(\omega_y - \omega_x)/2\pi = 2.6$ MHz, $\Delta\omega_L/2\pi = 100$ kHz, $\omega_0/2\pi = 1$ MHz, $T_s = 80$ ps, and $\eta = 2.0$.

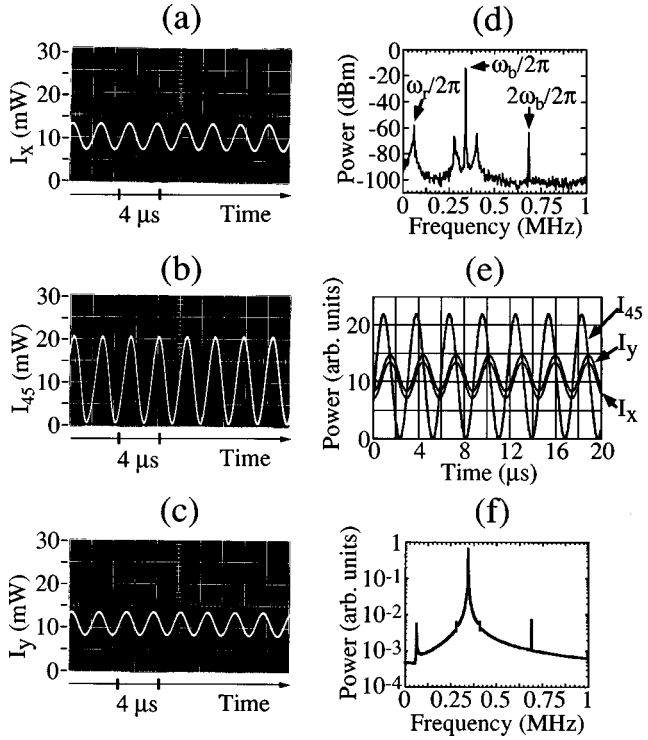

FIG. 3. Same as Fig. 2 with $(\omega_y - \omega_x)/2\pi = 357$ kHz.

on the photodiode the temporal evolutions of the intensities along the x [Fig. 2(a)] and y [Fig. 2(c)] directions and their beat note at $\omega_b/2\pi = (\omega_+ - \omega_-)/2\pi \approx 2.6$ MHz [Fig. 2(b)] with the polarizer aligned at 45° of the x and y directions. We check that since $|\omega_y - \omega_x| \gg \Delta\omega_L$, the eigenstates are almost perfectly x- and y-linearly polarized. However, we observe small modulations of their output powers at the beat frequency. The beat note of Fig. 2(b) is then sent to a spectrum analyzer and the corresponding power spectrum is displayed in Fig. 2(d). The undamped relaxation oscillation can be seen in this spectrum, together with the sidebands it induces in the power spectrum of the beat note at 2.6 MHz. With the parameters corresponding to the experimental results of Figs. 2(a)–2(d), we numerically integrate Eqs. (12) and (13). We then obtain the results of Figs. 2(e) and 2(f), which are in very good agreement with the experiment. In particular, the modulations of the intensities I_x and I_y are well reproduced, and the residual peak at the frequency $\omega_r/2\pi = 65$ kHz of relaxation oscillations can be seen in the spectrum of Fig. 2(f). Figure 2 provides evidence of the classical beat note between the two cold-cavity eigenstates, contrary to the following results which are no longer usual.

As expected from Eq. (2), the adjustment of $\Delta\varphi$ allows the precise and continuous control of the eigenfrequency difference $\omega_+ - \omega_-$. When this frequency difference is decreased, we can expect the two eigenstates to become slightly elliptical and to experience more nonlinearities as the relaxation oscillation frequency is approached. We set this frequency difference to $\omega_b/2\pi = 343$ kHz. We then observe the intensity evolutions of the laser output through the polarizer aligned with the x [Fig. 3(a)] and y [Fig. 3(c)] axes and at 45° of the x axis [Fig. 3(b)]. As expected, it appears that the intensities observed with the polarizer aligned along the x or the y axis are now strongly modulated at the beat frequency [see Figs. 3(a) and 3(c)]. The spectrum of the signal delivered by the photodiode and corresponding to Fig. 3(b) is shown in Fig. 3(d). One recognizes the undamped relaxation oscillation frequency at 65 kHz, and the beat note at 343 kHz together with its relaxation oscillation induced sidebands. Also present is the first harmonic of the beat note at 686 kHz. The theoretical results corresponding to this experiment are given in Figs. 3(e) and 3(f). One can see that the intensities as well as the spectrum are very well reproduced by the numerical integration of Eqs. (12) and (13). Note that the ratio of the powers at angular frequencies ω_b and $2\omega_b$ obtained experimentally [Fig. 3(d)] is also well reproduced theoretically [Fig. 3(f)].

In the results of Figs. 2 and 3, the loss anisotropy is in first approximation negligible, and we just obtain the beating of the two eigenstates. Of course, due to competition effects, a close look at the very-low-intensity spectra of the two eigenstates leads to the observation of the well-known frequencies associated with antiphase dynamics between the two eigenstates [20]. We have also checked experimentally that, as in previous works, these frequencies vanish in the total intensity $I_x + I_y$ spectrum.

2. $\omega_r < \Delta\omega_L < 2\omega_r$

By further decreasing ω_b, we reach situations where the beat note of the preceding subsection is replaced by other types of behaviors. Indeed, this beat note becomes strongly perturbed when the angular eigenfrequency difference ω_b

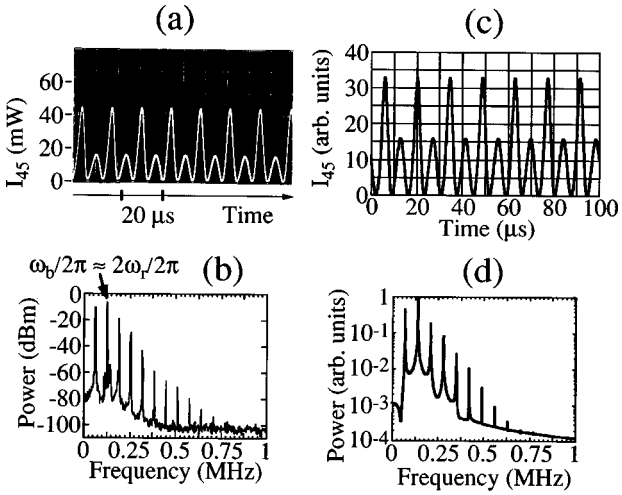

FIG. 4. (a) Experimental evolution of the component of the laser output power polarized at 45° of the x and y axes versus time. (b) Corresponding experimental spectrum. (c), (d) Corresponding theoretical results obtained with the same parameters as in Fig. 2 except $\Gamma_y/1.001=\Gamma_x=3.8\times10^7$ s^{-1} and $(\omega_y-\omega_x)/2\pi=165$ kHz.

meets the double of the relaxation oscillation angular frequency ω_r. The period of the output intensity modulation then doubles, as is shown in Fig. 4(a). The corresponding experimental spectrum is given in Fig. 4(b). The theoretical intensity temporal evolution [Fig. 4(c)] and spectrum [Fig. 4(d)] show remarkable agreement with the experimental ones. In this situation, the polarization of each eigenstate is elliptical and, whatever the orientation of the output polarizer, the same modulation wave form is observed experimentally and theoretically.

The next uncommon feature as we decrease the phase anisotropy $\Delta\varphi$ is observed when $\omega_y-\omega_x$ comes close to ω_r. Indeed, although this frequency difference is now smaller than the locking threshold $\Delta\omega_L$, suggesting that the cold-cavity eigenstates should be locked, *a distorted beat note still exists*, as is shown in Fig. 5(a) (temporal evolution of the intensity) and Fig. 5(b) (corresponding spectrum) at a beat frequency almost equal to the relaxation oscillation frequency ω_r. The corresponding theoretical calculations are reproduced in Figs. 5(c) and 5(d), in close agreement with

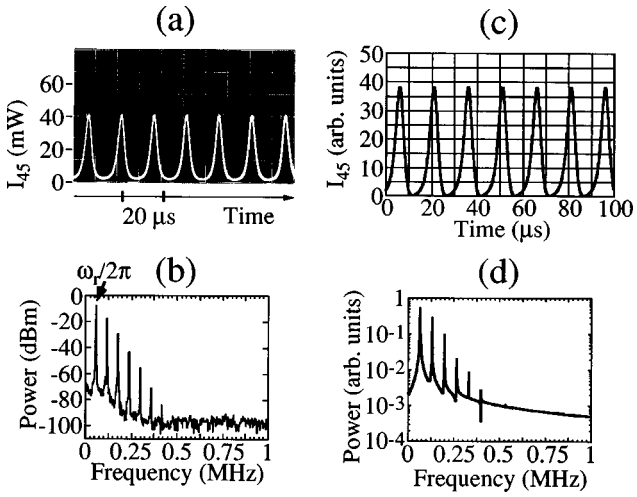

FIG. 5. Same as Fig. 4 with $(\omega_y-\omega_x)/2\pi=55$ kHz.

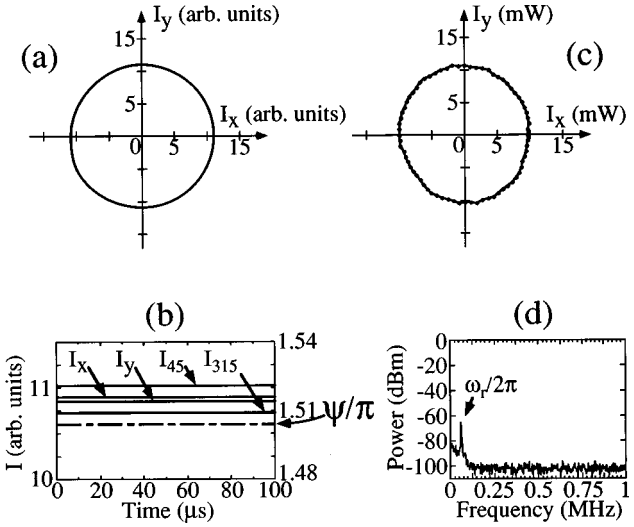

FIG. 6. Circularly polarized cw regime. (a) Theoretical polar plot of the intensity obtained with the same parameters as in Fig. 4, except $(\omega_y-\omega_x)/2\pi=80$ kHz. (b) Theoretical evolutions of the components of the laser output power (full line) and of the phase Ψ (dotted-dashed line) versus time. (c) Corresponding measured polarization ellipse. (d) Corresponding spectrum.

the experimental features. In particular, they confirm the fact that the x- and y-polarized components of the field are surprisingly unlocked ($\langle\dot{\Psi}\rangle\neq0$), although $|\omega_y-\omega_x|<\Delta\omega_L$. Besides, we find that both eigenstates then exhibit the same intensity evolution.

However, for other values of $\omega_y-\omega_x$ smaller than the locking threshold $\Delta\omega_L$, it eventually happens that the two eigenstates lock to the same frequency. Then, a peculiar oscillation regime appears. Namely, only one mode oscillates in a cw regime with a quasicircular polarization. The calculated temporal evolutions of the intensities and the phase Ψ are given in Fig. 6(b), leading to the expected polarization ellipse reproduced in Fig. 6(a). The laser output power is perfectly continuous, for any considered polarization direction. The evolution of the corresponding phase difference, shown in Fig. 6(b), provides evidence of the circularity of the emitted field polarization ($\Psi\approx3\pi/2$). In this situation, the experimental polarization has been checked to be circular, by measuring the output power while rotating the polarizer located in front of the detector [see Fig. 6(c)]. It is also proved that the laser is then purely monomode, since the beat note has vanished in the power spectrum [see Fig. 6(d)]. Moreover, we check experimentally and theoretically that the handedness of the output polarization can be reversed by changing the sign of $\omega_y-\omega_x$.

3. $\omega_r\ll\Delta\omega_L$

When the locking range is further increased, so that $\omega_r\ll\Delta\omega_L$, new temporal evolutions of the intensity are observed. Far from the locking range, i.e., when $\Delta\omega_L\ll\Delta\omega_b$, the usual beat note is observed experimentally as well as predicted theoretically (the results are qualitatively similar to the ones obtained in Figs. 2 and 3). Let us now turn to the opposite situation where $|\omega_y-\omega_x|<\Delta\omega_L$, i.e., when the frequencies of the two eigenstates of the cold cavity are locked. Then, if the laser behavior followed the predictions of the

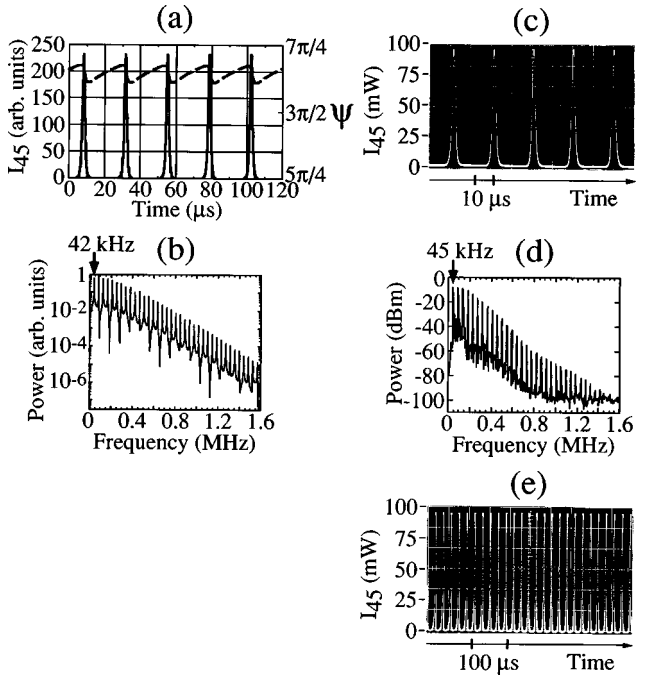

FIG. 7. Single-pulse regime. (a) Theoretical evolutions of the component of the laser output power (full line) polarized at 45° of the x and y axes and of the phase Ψ (dashed line) versus time, obtained with the same parameters as in Fig. 2, except $(\omega_y-\omega_x)/2\pi=500$ kHz and $\Delta\omega_L/2\pi=1.24$ MHz. (b) Corresponding theoretical spectrum. (c)–(e) Corresponding experimental results. Notice the theoretical as well as experimental increase of the laser peak power with respect to the results of Fig. 2.

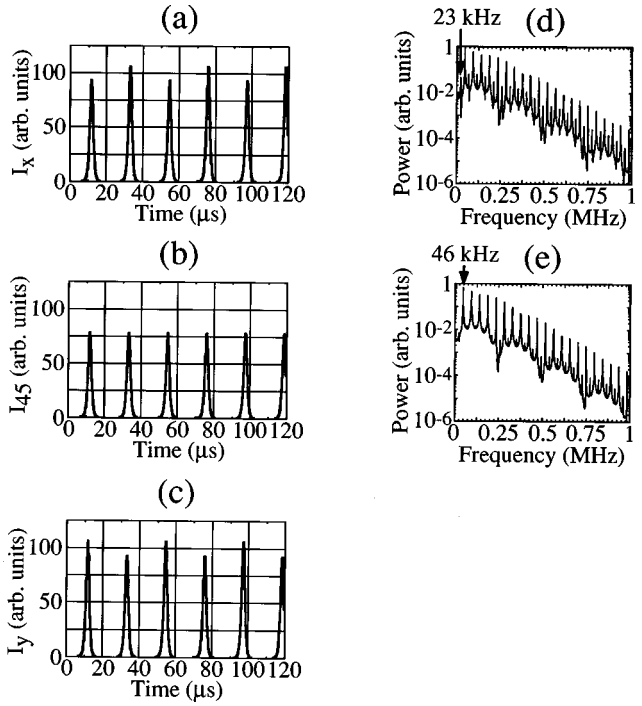

FIG. 8. Theoretical double-pulse regime. (a)–(c) Theoretical evolutions of the component of the laser output power polarized (a) along the x axis, (b) at 45° of the x and y axes, (c) along the y axis versus time, obtained with the same parameters as in Fig. 4, except $(\omega_y-\omega_x)/2\pi=200$ kHz and $\Delta\omega_L/2\pi=500$ kHz. (d), (e) Theoretical spectra corresponding to (a), (b).

cold cavity summarized in Fig. 1(b), we would expect only one of the eigenstates to oscillate continuously, with its polarization elliptical and roughly aligned with the low loss axis of the loss anisotropy $\Delta t_\perp$. However, Eqs. (12) and (13) exemplify the predominant role of the active medium in the laser behavior. In particular, they stress the role of the different components of the population inversion, whose decay time is much longer than the empty cavity decay time. We can thus expect the relaxation oscillation phenomena to play a predominant role. This is illustrated by the predictions of Figs. 7(a) and 7(b), which have been obtained for $(\omega_y-\omega_x)/2\pi=500$ kHz and $\Delta\omega_L/2\pi=1.24$ MHz. Figure 7(a) shows that the frequency locking of the two eigenstates $(\langle\dot{\Psi}\rangle=0)$ leads to an interesting self-pulsing operation of the laser, the pulse duration being of the order of 2 μs, and its polarization being elliptical. To check this prediction experimentally, we further tilt the intracavity étalon in order to increase the locking threshold $\Delta\omega_L$. For $|\omega_y-\omega_x|<\Delta\omega_L$, we then obtain the experimental results of Figs. 7(c)–7(e), which confirm the predictions of this new pulsed regime. In particular, Fig. 7(e) shows that such a regime is not due to spiking effects related to the onset of lasing, but is a very stable pulsed oscillation regime. We check experimentally that the pulses are elliptically polarized, and that their duration is equal to 2 μs, as expected. It is worth noting that since the phase difference Ψ between the x- and y-polarized components of the laser field is locked, this operation regime of the laser can really be called monomode [14], contrary to the usual pulsed phase locking in multimode lasers [25,26].

Besides, it is striking to notice that the repetition rate of the laser pulses is approximately equal to 45 kHz, both theoretically and experimentally, a value slightly below the relaxation oscillation frequency (65 kHz). This repetition rate can be varied within a few kHz around this value by careful adjustment of the phase and loss anisotropies. Moreover, we observe experimentally that the repetition rate increases with the excitation rate η of the laser. These results and the fact that the pulsed regime is experimentally and theoretically obtained only for $\omega_r<\omega_y-\omega_x<\Delta\omega_L$ definitely prove that this new pulsed regime is due both to the frequency locking of the two eigenstates of the cold cavity, and to the existence of relaxation oscillations, i.e., to the fact that the population inversion cannot be eliminated adiabatically in Eqs. (12).

Contrary to the latter situation where the intensity evolutions along x and y axes are identical, a slight reduction of the loss and phase anisotropies leads to a double-pulsed regime where the intensities along x and y axes exhibit complementary evolutions. Indeed, when now $(\omega_y-\omega_x)/2\pi=200$ kHz and $\Delta\omega_L/2\pi=500$ kHz, numerical integration of Eqs. (12) and (13) yields the predictions depicted in Fig. 8. One can observe that, although the intensity along the 45° direction [Fig. 8(b)] has a single-pulse temporal behavior with a 46-kHz repetition rate [see the spectrum in Fig. 8(e)], the intensities along the x [Fig. 8(a)] and y [Fig. 8(c)] directions now exhibit a double-pulsed oscillation regime. The fundamental frequency of the intensity spectrum is then 23 kHz [see the spectrum in Fig. 8(d)]. To verify this prediction experimentally, we tilt the intracavity étalon back in order to decrease the locking threshold $\Delta\omega_L$. We then obtain the experimental results of Fig. 9, which confirm the

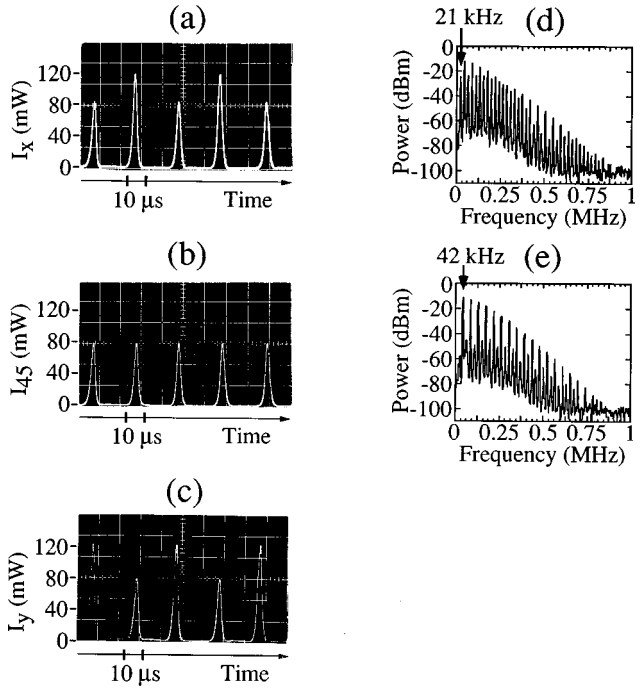

FIG. 9. Experimental double-pulse regime. (a)–(c) Experimental evolutions of the component of the laser output power polarized (a) along the x axis, (b) at 45° of the x and y axes, (c) along the y axis versus time, corresponding to the theoretical predictions of Fig. 8. (d), (e) Experimental spectra corresponding to (a), (b). Notice the vanishing of the lowest-frequency component when the polarizer is aligned at 45° to the x axis.

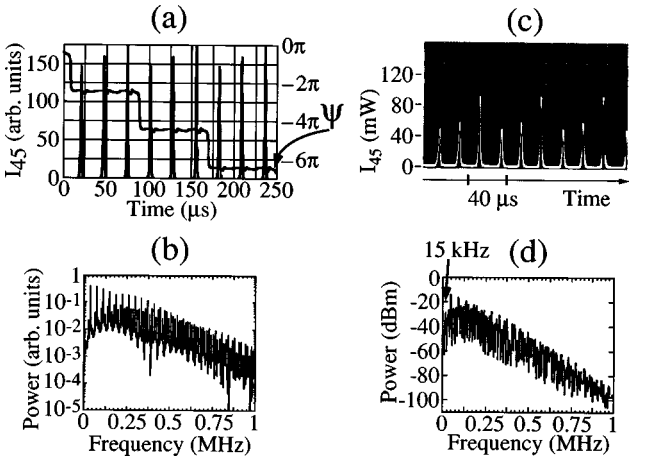

FIG. 10. Triple-pulse regime. (a) Theoretical evolutions of the component of the laser output power polarized at 45° of the x and y axes and of Ψ versus time, obtained with the same parameters as a in Fig. 4, except $\Gamma_y/1.1=\Gamma_x=3.8\times10^7\ \mathrm{s}^{-1}$, $(\omega_y-\omega_x)/2\pi=500$ kHz, and $\Delta\omega_L/2\pi=744$ kHz. (b) Corresponding theoretical spectrum. (c), (d) Corresponding experimental results. The I_x and I_y components of the output light (not shown) exhibit the same temporal behavior as I_{45}.

predictions of a double-pulsed regime along the x and y directions. Note that, as predicted, the intensity evolutions observed with the polarizer aligned along the x and y directions are complementary and that the intensity detected with the polarizer aligned at 45° of the x and y axes exhibits single pulses at 42 kHz [Figs. 9(b) and 9(e)], as expected from Figs. 8(b) and 8(e).

Finally, when the loss anisotropy $\Delta t_\perp$ is accompanied by a loss anisotropy aligned with the x and y directions ($\Gamma_x\neq\Gamma_y$), the numerical integration of Eqs. (12) and (13) leads to the prediction of phase-locked multiple-pulse oscillation regimes with still lower fundamental frequencies. For example, Figs. 10(a), and 10(b) show the theoretical temporal evolution of the intensity as well as the low-frequency spectrum when $(\omega_y-\omega_x)/2\pi=500$ kHz, $\Delta\omega_L/2\pi=744$ kHz, and $\Gamma_y/\Gamma_x=1.1$. This triple-pulsed oscillation regime is also obtained experimentally, as checked in Figs. 10(c) and 10(d). Note that, here again, the phases are locked and the laser is consequently monomode with an elliptical polarization.

4. Towards shorter pulses?

The preceding results have stressed the fact that the repetition rate of the monomode phase-locked single-pulsed regime is closely related to the frequency of relaxation oscillations. This peculiar oscillation regime could lead to interesting applications to the design of a new type of pulsed lasers, provided that the pulse duration could be reduced by increasing ω_r. To test this idea, we increase ω_r by reducing the cavity length to $L=0.105$ m and increasing η to 3.1. Then, when unlocked, the laser output power is 28 mW and its relaxation oscillation frequency is $\omega_r/2\pi=157.5$ kHz, leading to $\Gamma_x=\Gamma_y=1.07\times10^8\ \mathrm{s}^{-1}$. With these parameters and with $(\omega_y-\omega_x)/2\pi=6.15$ MHz and $\Delta\omega_L/2\pi=6.82$ MHz, Eqs. (12) and (13) lead to the predictions of Figs. 11(a)–11(c). We then expect a pulse width of the order of 720 ns and a repetition rate larger than 100 kHz. This is verified experimentally, as can be seen in Figs. 11(d)–11(f). In particular, pulse durations as low as 780 ns are obtained in this case, showing that increasing ω_r permit us (i) to increase the repetition rate of the pulses and (ii) to reduce their durations. In order to further reduce the pulse duration, we can imagine using microchip lasers with controlled anisotropies. With $L=1$ mm and $\eta=3$, the relaxation oscillation frequency must be $\omega_r/2\pi=1.573$ MHz, leading to $\Gamma_x=\Gamma_y=1.124\times10^{10}\ \mathrm{s}^{-1}$. Then, with $(\omega_y-\omega_x)/2\pi=3$ MHz and $\Delta\omega_L/2\pi=478$ MHz, our model predicts the pulses shown in Fig. 12. The pulse duration, which is now predicted to be 60 ns, becomes almost as short as in the case of passively Q-switched microchip lasers, without the need of an intracavity saturable absorber. Moreover, as can be seen from Fig. 12(a), the repetition rate is now 920 kHz, a value larger than the repetition rates which can be reached with comparable passively Q-switched microchip Nd:YAG lasers.

IV. CONCLUSION

We have experimentally investigated the dynamics of the two eigenstates of a longitudinally monomode quasi-isotropic solid-state laser in the presence of crossed phase and loss linear anisotropies. We have developed a theoretical model for such lasers, taking the cold-cavity locking region into account. Starting from the density matrix formalism, we have derived the coupled differential equations governing the amplitudes and phases of two laser eigenstates, as well as the population inversion in the active medium. The vectorial nature of the atom-field interaction appears through an angular Fourier expansion of the population inversion. The resulting six differential equations are applied to describe the temporal

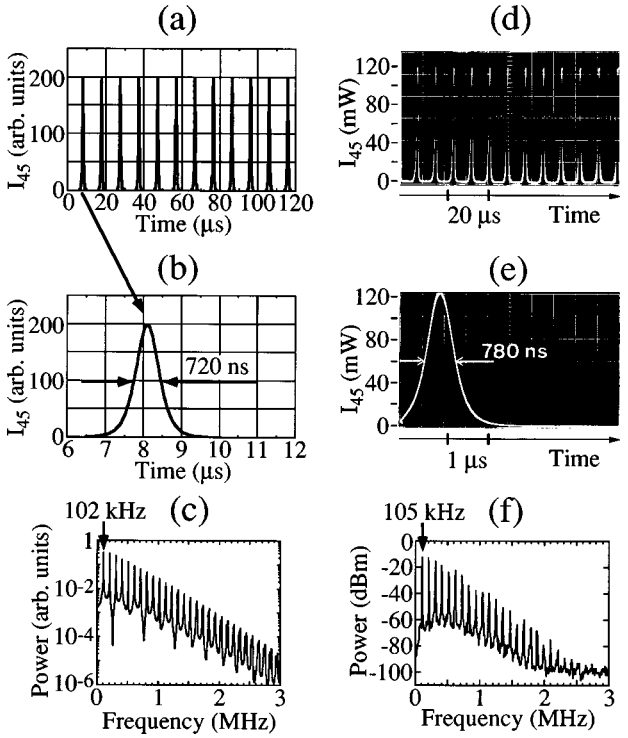

FIG. 11. Single-pulse regime for a short cavity ($L=0.105$ m). (a) Theoretical evolution of the component of the laser output power polarized at 45° of the x and y axes versus time, obtained with $\eta=3.1$, $L=0.105$ m, $\Gamma_y/1.001=\Gamma_x=1.07\times10^8$ s^{-1}, $(\omega_y-\omega_x)/2\pi=6.15$ MHz, and $\Delta\omega_L/2\pi=6.82$ MHz. (b) Zoom on one of the pulses of (a), showing a pulse width equal to 720 ns FWHM. (c) Corresponding theoretical spectrum. (d)–(f) Corresponding experimental results. The I_x and I_y components of the output light (not shown) exhibit the same temporal behavior as I_{45}.

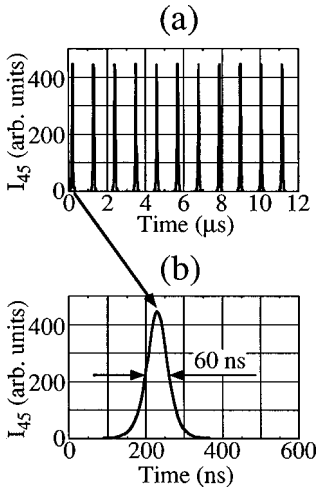

FIG. 12. Single-pulse regime predicted for a very short cavity ($L=1$ mm). (a) Theoretical evolution of the component of the laser output power polarized at 45° of the x and y axes versus time, obtained with $\eta=3$, $L=1$ mm, $\Gamma_y/1.001=\Gamma_x=1.124\times10^{10}$ s^{-1}, $(\omega_y-\omega_x)/2\pi=3$ MHz, and $\Delta\omega_L/2\pi=478$ MHz, leading to a repetition rate of 920 kHz. (b) Zoom on one of the pulses of (a), showing a pulse width equal to 60-ns FWHM.

behavior of a quasi-isotropic solid-state laser with a very short active medium and containing crossed phase and loss anisotropies.

New behaviors in the laser output intensity and polarization are then observed in a diode-pumped longitudinally and transversely monomode Nd:YAG laser sustaining the oscillation of two polarization eigenstates.

(i) When the locking range is of the order of the relaxation oscillation frequency of the laser, a usual beat note is observed between the two cold-cavity eigenstates, except for particular values of the angular beat frequency of the system, namely, ω_r and $2\omega_r$, which lead to original behaviors.

(ii) When the locking range is slightly larger than the relaxation oscillation frequency of the laser, a monomode continuous-wave circularly polarized regime is observed as soon as the cold-cavity eigenfrequency difference falls within the locking region.

(iii) When the relaxation oscillation frequency of the laser is small with respect to the locking bandwidth, different specific self-pulsed regimes are observed. Multiple or single pulses are shown to be emitted with pulse widths as short as 780-ns full width at half maximum (FWHM) at a repetition rate slightly smaller than the relaxation oscillation frequency and peak powers about ten times the corresponding cw power.

All these observations are theoretically confirmed by our model. Depending on the magnitude of the loss and phase anisotropies, every observed regime has been theoretically reproduced. Usual as well as distorted beat notes between the two eigenstates, cw circular polarization emission, and single and multiple pulsing in the self-locked regime are numerically obtained. The single-pulse regime is obtained (i) at a repetition rate of about 42 kHz, with a pulse width of 2 μs and a peak power of 20 times the cw output power, and (ii) at a repetition rate of about 105 kHz with a pulse width of 720 ns depending mainly on the frequency of relaxation oscillations. We have consequently verified that the reduction of the photon lifetime in the cavity leads to shorter pulses emitted with a higher repetition rate, as observed. This opens the possibility of generating nanosecond pulses at MHz repetition rates when using microchip lasers, without Q-switching processes. Furthermore, we have checked experimentally the appearance of such self-pulsed regimes in a compact Er:Yb:glass laser emitting at 1.55 μm.

To conclude, the introduction of a crossed loss anisotropy creating a locking region for the two eigenstates of a monomode solid-state laser has led to the observation of peculiar temporal behaviors for the output intensity, which are theoretically confirmed. These behaviors are physically explained by the nonlinear interaction between two orthogonal eigenstates in the active medium of lasers where the photon lifetime in the cavity is much shorter than the population inversion lifetime (class-B lasers). The role of the relaxation oscillations, as well as the need for a self-locking region, have been stressed. Besides, the self-pulsed monomode output may prove very useful when shorter laser cavities are used. Moreover, the possible existence of regions of chaotic behavior that we can suspect from preliminary theoretical and experimental observations deserves further investigations.

ACKNOWLEDGMENTS

The authors are happy to thank J. Marty and E. Molva for providing the microlaser used in the experiments. This work was partially supported by the Conseil Régional de Bretagne.

[1] H. Statz and G. de Mars, in *Quantum Electronics*, edited by C. H. Townes (Columbia University, New York, 1960), p. 650.
[2] C. L. Tang, H. Statz, and G. de Mars, J. Appl. Phys. **34**, 2289 (1963).
[3] P. Mandel, K. Otsuka, J.-Y. Wang, and D. Pieroux, Phys. Rev. Lett. **76**, 2694 (1996).
[4] A. Owyoung and P. Esherick, Opt. Lett. **12**, 999 (1987).
[5] S. P. Bush, P. F. Mead, and C. C. Davis, in *IEEE/Lasers and Electro-Optics Society 1991 Annual Meeting*, San Jose, CA, November 1991 (IEEE/LEOS, Piscataway, NJ, 1991), p. 55.
[6] C. He and D. K. Killinger, Opt. Lett. **19**, 396 (1994).
[7] J. W. Czarske and H. Mueller, Opt. Commun. **114**, 223 (1995).
[8] G. W. Baxter, J. M. Dawes, P. Dekker, and D. S. Knowles, IEEE Photonics Technol. Lett. **8**, 1015 (1996).
[9] M. Brunel, F. Bretenaker, and A. Le Floch, Opt. Lett. **22**, 384 (1997).
[10] M. Brunel, O. Emile, F. Bretenaker, A. Le Floch, B. Ferrand, and E. Molva, Opt. Rev. **4**, 550 (1997).
[11] P. Nerin, P. Puget, P. Besesty, and G. Chartier, Electron. Lett. **33**, 491 (1997).
[12] M. Brunel, M. Vallet, A. Le Floch, and F. Bretenaker, Appl. Phys. Lett. **70**, 2070 (1997).
[13] P. Dekker and J. M. Dawes, J. Opt. Soc. Am. B **15**, 247 (1998).
[14] M. Brunel, O. Emile, M. Alouini, A. Le Floch, and F. Bretenaker, Opt. Lett. (to be published).
[15] H. Zeghlache and A. Boulnois, Phys. Rev. A **52**, 4229 (1995).
[16] P. Khandokhin, Ya Khanin, Yu Mamaev, N. Milovsky, E. Shirokov, S. Bielawski, D. Derozier, and P. Glorieux, Quantum Semiclassic. Opt. **10**, 97 (1998).
[17] P. Mandel, C. Etrich, and K. Otsuka, IEEE J. Quantum Electron. **QE-29**, 836 (1993).
[18] L. A. Lugiato, K. Wang, and Y. Sun, Opt. Commun. **105**, 397 (1994).
[19] W. H. Press, B. P. Flannery, S. A. Teukolsky, and W. T. Vetterling, *Numerical Recipes in Pascal* (Cambridge University Press, Cambridge, England, 1989), Chap. 15.
[20] S. Bielawski, D. Derozier, and P. Glorieux, Phys. Rev. A **46**, 2811 (1992).
[21] E. Lacot and F. Stoeckel, J. Opt. Soc. Am. B **13**, 2034 (1996).
[22] D. E. McCumber, Phys. Rev. **141**, 306 (1966).
[23] A. E. Siegman, *Lasers* (University Science, Mill Valley CA, 1986), Chap. 25, p. 962.
[24] A linear stability analysis of Eqs. (12) and (13) also yields the standard relation for the relaxation oscillation frequency given by Eq. (15), as far as the loss anisotropy is neglected.
[25] M. Sargent III, M. O. Scully, and W. E. Lamb, Jr., *Laser Physics* (Addison-Wesley, Reading MA, 1974), Chap. 9.
[26] P. W. Smith, Proc. IEEE **58**, 1342 (1970).